

Two-photon dynamics in coherent Rydberg atomic ensemble

Bing He,^{1,2} A. V. Sharypov,^{3,4} Jiteng Sheng,² Christoph Simon,¹ and Min Xiao^{2,5,*}

¹*Institute for Quantum Science and Technology, University of Calgary, Calgary, Alberta T2N 1N4, Canada*

²*Department of Physics, University of Arkansas, Fayetteville, AR 72701, USA*

³*Kirensky Institute of Physics, 50 Akademgorodok, Krasnoyarsk, 660036, Russia*

⁴*Siberian Federal University, 79 Svobodny Av., Krasnoyarsk, 660041, Russia*

⁵*National Laboratory of Solid State Microstructures and Department of Physics, Nanjing University, Nanjing 210093, China*

The process of two independent single-photon pulses interacting via Rydberg atomic ensemble under electromagnetically induced transparency condition is a completely dynamical one characterized by the time-dependent absorption, interaction strength and pulse group velocity. In addition to applying a numerical method to simulate such pulse motion with no steady state, we illustrate how the photons interact and propagate in the medium as well as the associated effects when they enter the Rydberg blockade and superluminal regime. The obtained photon motion is combined with the many-body dynamics for the whole pulses to find the real-time evolution of the pulses' quantum states. Our study presents a realistic picture of the dynamical process.

Strong nonlinearity at the single-photon level is desirable to the realization of all-optical quantum devices. Ensembles of highly excited Rydberg atoms under electromagnetically induced transparency (EIT) condition combine the advantages of strong atom-field coupling without significant absorption and non-local atomic interaction, and have attracted intensive experimental [1–7] and theoretical studies [8–16] recently. The strong correlation directly between single photons inside Rydberg atomic ensemble was observed [7], and the formation of a Wigner crystal of individual photons is also predicted [15]. When such interaction is applied to implement the cross-phase modulation (XPM) between two individual photons with a non-zero relative velocity as in Fig. 1 [17–20], a main difference from a single probe beam propagation in Rydberg EIT medium [1–16] is that no steady state exists for the pulses, because their interaction varies with the relative distance, pulse velocity that changes pulse sizes, as well as the absorption in medium. The previous

works have to approach the problem with the simplified pulse motion. For example, in [20], the pulse group velocity is assumed to take two constant values—the one under EIT condition and the speed of light c —across the boundary of Rydberg blockade region. The realistic time-dependence in the inherent nonlinear dynamics makes a complete solution of the problem rather challenging.

The detailed two-photon XPM via Rydberg EIT is as follows. One respectively couples the far-away input photons to cold Rydberg atoms under the EIT condition to form the light-matter quasi-particle called dark-state polariton (DSP) [21]. The spatial distribution of the pulses necessitates a quantum many-body description of the process. The prepared DSPs are in the state $|1\rangle_l = \int d^3x f_l(\mathbf{x}) \hat{\Psi}_l^\dagger(\mathbf{x}) |0\rangle$ for $l = 1, 2$, where $f_l(\mathbf{x})$ are their snapshots with $\int d^3x |f_l(\mathbf{x})|^2 = 1$, and $\hat{\Psi}(\mathbf{x}) = \cos\theta \hat{\mathcal{E}}(\mathbf{x}) - \sin\theta \hat{S}(\mathbf{x})$ is the DSP field operator. The many-body version of the atom-field Hamiltonian

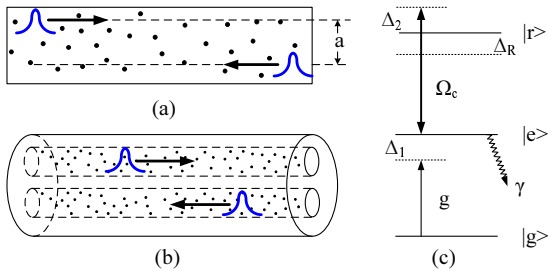


FIG. 1: (a) Two single photon pulses propagate in a Rydberg atomic ensemble. (b) Two pulses propagate in two parallel waveguides filled with Rydberg atoms. For the insignificant diffraction or the propagation in (b), the pulse profiles for our numerical simulation in Fig. 4 can be approximated as one-dimensional. (c) Atomic level scheme for the system. Without pulse interaction there is $\Delta_1 + \Delta_2 = 0$ under the EIT condition. Here $\Delta_1 = \omega_{eg} - \omega_p$, and $\Delta_2 = \omega_{re} - \omega_c$ (ω_c is the frequency of the pump beam). The Rydberg level is shifted by Δ_R due to the interaction with another pulse.

$$\begin{aligned}
 H_{AF}^l &= -\frac{1}{2} \int d^3x \{ \Omega_c \hat{S}_l^\dagger(\mathbf{x}) \hat{P}_l(\mathbf{x}) + g\sqrt{N} \hat{\mathcal{E}}_l^\dagger(\mathbf{x}) \hat{P}_l(\mathbf{x}) \\
 &+ H.c. \} + \int d^3x \Delta_1 \hat{P}_l^\dagger \hat{P}_l(\mathbf{x}) \\
 &= - \int d^3x \{ \omega^+ \hat{\Phi}_{+,l}^\dagger \hat{\Phi}_{+,l}(\mathbf{x}) + \omega^- \hat{\Phi}_{-,l}^\dagger \hat{\Phi}_{-,l}(\mathbf{x}) \} \quad (1)
 \end{aligned}$$

($\hbar = 1$) involving the electromagnetic field $\hat{\mathcal{E}}(\mathbf{x})$, the polarization field $\hat{P}(\mathbf{x}) = \sqrt{N} \hat{\sigma}_{ge}(\mathbf{x})$ and the Rydberg spin-wave field $\hat{S}(\mathbf{x}) = \sqrt{N} \hat{\sigma}_{gr}(\mathbf{x})$ can be diagonalized in terms of two bright-state polariton (BSP) fields $\hat{\Phi}_+(\mathbf{x}) = \sin\theta \sin\phi \hat{\mathcal{E}}(\mathbf{x}) + \cos\phi \hat{P}(\mathbf{x}) + \cos\theta \sin\phi \hat{S}(\mathbf{x})$ and $\hat{\Phi}_-(\mathbf{x}) = \sin\theta \cos\phi \hat{\mathcal{E}}(\mathbf{x}) - \sin\phi \hat{P}(\mathbf{x}) + \cos\theta \cos\phi \hat{S}(\mathbf{x})$, where their spectrum $\omega^\pm = \frac{1}{2}(\Delta_1 \pm \sqrt{\Delta_1^2 + g^2 N + \Omega_c^2})$ is a function of the input photon detuning Δ_1 , pump beam Rabi frequency Ω_c and atom density N . The combination coefficients for the polariton field operators satisfy the relations $\tan\theta = g\sqrt{N}/\Omega_c$ and $\tan 2\phi = \sqrt{g^2 N + \Omega_c^2}/\Delta_1$ with g as the atom-field coupling constant. When the

DSPs get close to each other, the interaction

$$H_I = \int d^3x d^3x' \hat{S}_1^\dagger(\mathbf{x}) \hat{S}_2^\dagger(\mathbf{x}') \Delta(\mathbf{x} - \mathbf{x}') \hat{S}_2(\mathbf{x}') \hat{S}_1(\mathbf{x}) \quad (2)$$

between the pulses takes effect. Here we consider the Van der Waals (VdW) potential $\Delta(\mathbf{x}) = -C_6/|\mathbf{x}|^6$ in Rydberg atomic ensemble. One wishes to perform an ideal XPM, $|1\rangle_1|1\rangle_2 \rightarrow e^{i\varphi}|1\rangle_1|1\rangle_2$, realizing a large and uniform phase φ through such interaction. The interaction, however, also causes the transition of DSP to BSPs containing $\hat{P}_l(\mathbf{x})$ components decaying at the rate γ . The decay of the $\hat{P}_l(\mathbf{x})$ field is described by [22]

$$H_D^l = i\sqrt{\gamma} \int d^3x \{ \hat{P}_l(\mathbf{x}) \hat{\xi}_l^\dagger(\mathbf{x}, t) - \hat{P}_l^\dagger(\mathbf{x}) \hat{\xi}_l(\mathbf{x}, t) \}, \quad (3)$$

with the white-noise operators of the reservoirs satisfying $[\hat{\xi}_l(\mathbf{x}, t), \hat{\xi}_l^\dagger(\mathbf{x}', t')] = \delta^3(\mathbf{x} - \mathbf{x}') \delta(t - t')$. The consequent pulse absorption from interaction indicates that the unitary evolution approach [17–19] to the two-photon process only reflects a partial reality. On the other hand, the nonlinear term in (2) makes it inappropriate to linearize the many-body dynamics of the non-local atomic interaction as in [20]. The purpose of the present work is to find a realistic picture of the dynamical process.

Before studying the input's quantum state evolution, one needs to ascertain the pulses' propagation in the medium, so that their interaction time should be known. The propagation of a pulse is determined by the response of the atoms it resides on. The atom-field coupling process on one of the atoms (note that Eq. (1) is about the whole ensemble) is described by the following equations for the elements of the atomic density matrix [23]:

$$\dot{\rho}_{re} = -\left(\frac{\gamma_{re}}{2} + i(\Delta_2 + \Delta_R)\right) \rho_{re} + i\Omega_c(\rho_{rr} - \rho_{ee}) + i\mu_{eg} E_p^* \rho_{rg}, \quad (4a)$$

$$\dot{\rho}_{eg} = -\left(\frac{\gamma_{eg}}{2} + i\Delta_1\right) \rho_{eg} + i\mu_{eg} E_p(\rho_{ee} - \rho_{gg}) - i\Omega_c \rho_{rg}, \quad (4b)$$

$$\dot{\rho}_{rg} = -\left(\frac{\gamma_{rg}}{2} + i(\Delta_1 + \Delta_2 + \Delta_R)\right) \rho_{rg} - i\Omega_c \rho_{eg} + i\mu_{eg} E_p \rho_{re}, \quad (4c)$$

where μ_{ij} are the transition dipole matrix elements and γ_{ij} the decay rates of the relevant levels, with $\gamma_{eg} = \gamma$ and $g^2 = \mu_{eg}^2 \omega_p / \epsilon_0$ (ω_p is the input pulses' central frequency). The interaction with another pulse shifts the energy of the level $|r\rangle$ and hence adds an extra term $\Delta_R = \sin^2 \theta T(t) \int d^3x' \Delta(\mathbf{x} - \mathbf{x}') \langle \hat{\Psi}^\dagger \hat{\Psi} \rangle(\mathbf{x}', t)$ to the detuning Δ_2 of the pump beam. Here we consider the time-dependent transmission rate $T(t)$ and the time-varying pulse distribution $\langle \hat{\Psi}^\dagger \hat{\Psi} \rangle(\mathbf{x}, t)$. With the weak amplitude E_p of the single photons one has

$$\begin{pmatrix} \rho_{eg}(t) \\ \rho_{rg}(t) \end{pmatrix} = -i\mu_{eg} \int_0^t d\tau e^{\int_\tau^t dt' \hat{M}(t')} \begin{pmatrix} E_p \\ 0 \end{pmatrix} \quad (5)$$

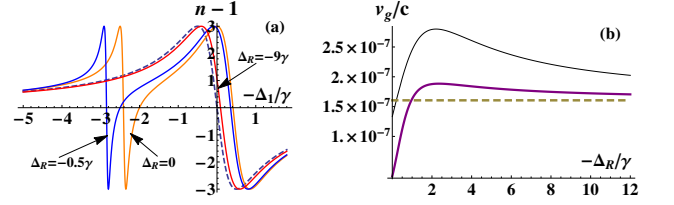


FIG. 2: (a) Shift of refractive index curves with increasing negative Δ_R . Here $n - 1 = \text{Re}\{\chi^{(1)}\}$ is obtained from the approximated solution to (4a)-(4c) in slow light regime, and we take the photon detuning $\Delta_1 = 2\gamma$, its initial group velocity $v_g = 10\text{m/s}$, and the pump Rabi frequency $\Omega_c = \gamma$. The excited level $|e\rangle$ is $5P_{1/2}$ of ^{87}Rb . The dashed curve is that for the two level system of the corresponding parameters. The minus sign of the horizontal axes label comes from our definition of Δ_1 . (b) Group velocity v_g vs Δ_R . The thicker solid curve is for $\Omega_c = \gamma$, while the thinner is about $\Omega_c = 2\gamma$. The dashed line is the group velocity of the corresponding two-level system.

from (4a)-(4c), where

$$\hat{M}(t) = \begin{pmatrix} -\left(\frac{\gamma}{2} + i\Delta_1\right) & -i\Omega_c \\ -i\Omega_c & -\frac{\gamma_{rg}}{2} - i(\Delta_1 + \Delta_2 + \Delta_R(t)) \end{pmatrix}.$$

It is straightforward to obtain the time-dependent refractive index and decay rate from the susceptibility $\chi^{(1)}(t) = -N\mu_{eg}\rho_{eg}(t)/(\epsilon_0 E_p)$ based on (5).

When two pulses approach each other, one phenomenon that could happen is known as Rydberg blockade. For the red-detuned photons ($\Delta_1 > 0$) the rising magnitude of negative Δ_R constantly shifts the refractive index curve going through the EIT point at a certain detuning Δ_1 toward that of the corresponding two-level system. In the limit $|\Delta_R| \gg \gamma$ the system will virtually turn into a two-level one; see Fig. 2(a). One signature of Rydberg blockade is a platform of nearly unchanging group velocity shown in Fig.2(b). A stronger pump beam can offset the blockade effect and push the platform to larger $|\Delta_R|$. In the blockade regime the pulse group velocity asymptotically tends to that of the corresponding

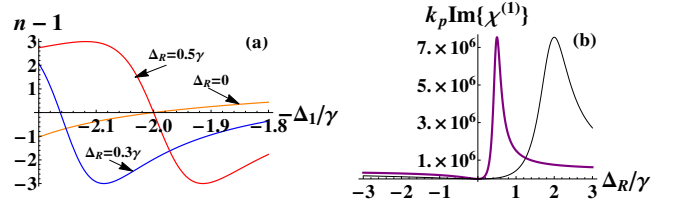


FIG. 3: (a) Shift of refractive index curves with increasing positive Δ_R for the system in Fig. 2. The gradient of the refractive index curve at $\Delta_1 = 2\gamma$ gradually becomes negative, implying negative group velocity in the superluminal regime. (b) Pulse damping rate $\frac{\omega_p}{c} \text{Im}\{\chi^{(1)}\}$ in the unit of m^{-1} as function of Δ_R . The thicker curve is for $\Omega_c = \gamma$ and the thinner for $\Omega_c = 2\gamma$. The damping rate curves will tend to the value of the corresponding two level system with $\Delta_R \rightarrow \pm\infty$.

two-level system; only those with $\Delta_1 \leq 0.5\gamma$ in Fig. 2 can reach the speed of light c with growing negative Δ_R .

The breaking of the perfect EIT condition by the interaction induced detuning Δ_R certainly causes dissipation. Interestingly, shown in Fig.3, the consequent pulse absorption is asymmetric with respect to the sign of gradually increasing Δ_R . The pulses will enter the superluminal regime accompanied by a huge damping, if the signs of Δ_1 and Δ_R are the same. Under the attractive VdW potential this danger exists for two blue-detuned photons that gradually get close with time [24].

We now consider two red-detuned photons coupled to ensemble and propagating toward each other. As the pulses get closer, they will expand spatially because the characteristic size of their distribution $\langle \hat{\Psi}_l^\dagger \hat{\Psi}_l \rangle(\mathbf{x}, t)$ is proportional to $v_g(t)$. This modifies the Δ_R calculated with the relative distance and absorption of the pulses, which constantly keep changing as well. We use a numerical algorithm to simulate this dynamical process. From the coordinate origin $Z = 0$ situated on the center of one pulse, the longitudinal relative distance $-L \leq Z \leq L$ to the other pulse's center throughout their motion is divided into n_d grids. The detuning Δ_R at the i -th ($0 < i \leq n_d - 1$) position is calculated with the pulse size and transmission rate at the $i - 1$ -th position. Together with the obtained numerical values of Δ_R at the previous positions of $0 \leq k \leq i - 1$, it is plugged into (5) for the numerical integral to find the susceptibility $\chi^{(1)}$. In the same way the updated group velocity and transmission rate from the susceptibility at the position i will be used to calculate the Δ_R at the $i + 1$ -th position. Running the iterative procedure with sufficiently large grid number n_d approaches the real pulse motion.

Figure 4 illustrates an example of pulse motion found by the above mentioned numerical method. As shown in Fig.4(a) and 4(b), the greater interaction between more transversely adjacent pulses is inseparable with the more significant pulse losses. In where Rydberg blockade starts to manifest, the accumulated pulse absorption has been harmful to the survival of the interacting photons (see Fig.4(b) and 4(c)). The pulse damping can be lowered by choosing a higher detuning Δ_1 , but the trade-off is to require a narrower pulse bandwidth (correspondingly a longer pulse size) to fit into the smaller EIT transparency window, incurring a more prominent effect measured by the ratio $\delta_v(Z) = |\{v_g(Z, \sigma(Z)) - v_g(Z, 0)\} / v_g(Z, 0)|$ shown in Fig.4(d). Here $v_g(Z, \sigma(Z))$ is the group velocity at the location of the characteristic longitudinal size $\sigma(Z)$ from the pulse center, and $v_g(Z, 0)$ is that at the pulse center. The non-zero quantity δ_v means the pulses' non-uniform group velocity distribution in the co-moving coordinate with the pulse centers, which is equivalent to a group velocity dispersion that could make the pulses totally disappear even without absorption. Moreover, if the pulse size σ is too large, the detuning Δ_R (proportional to $1/\sigma^6$ due to pulse distribution) over the pulses

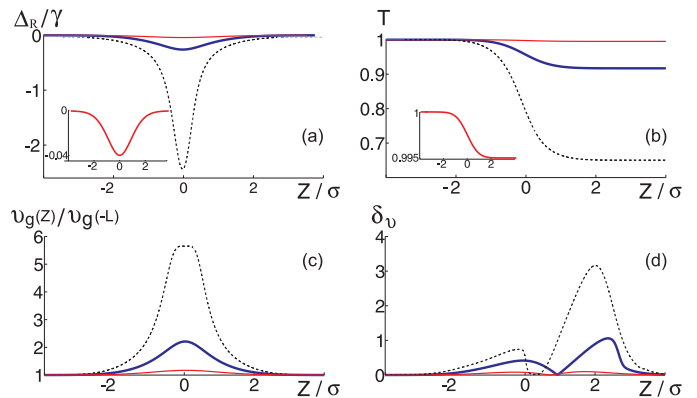


FIG. 4: Numerical simulation for pulse motion. We use $|g\rangle = 5S_{1/2}$, $|e\rangle = 5P_{1/2}$, and $|r\rangle = 82D_{3/2}$ of ^{87}Rb , with the VdW coefficient $|C_6| = 8500 \text{ GHz} \cdot \mu\text{m}^6$ [25] and $\gamma = 2\pi \cdot 5.75 \text{ MHz}$. The system parameters are chosen as $Ng^2/\Omega_c^2 = 3 \cdot 10^7$ ($v_g(-L) = 10 \text{ m/s}$), $\Omega_c = \gamma$, and $\Delta_1 = -\Delta_2 = 2\gamma$. The input Gaussian shaped pulses with $f(z) = (\frac{1}{\sqrt{\pi}\sigma})^{\frac{1}{2}} e^{-\frac{1}{2}z^2/\sigma^2}$ have the initial size $\sigma = 11.1 \mu\text{m}$, with the corresponding bandwidth well fitted into the EIT window. The dashed curves are about the transverse separation $a = 0.58 \sigma$, the thicker solid ones for $a = \sigma$, and the thinner solid ones for $a = 1.5 \sigma$. The iterative step size for the numerical simulation is 0.005σ . Here we neglect the Doppler effect, since the pulse interaction for $a = 0.58 \sigma$ accelerates the Rubidium atoms only to the order of 10^{-4} m/s . (a) Interaction induced $\Delta_R(Z)$ at pulse centers. The insertion is the refined plot for $a = 1.5 \sigma$. (b) Transmission rate $T(Z) = \exp(-k_p \int_{-L}^Z dy \text{Im}\{\chi^{(1)}(y)\})$. (c) Group velocity $v_g(Z) = c/n_g$ at pulse centers. Here $n_g(Z) = n(Z) + \omega_p \partial n(Z) / \partial \omega_p$. The most transversely adjacent situation shows a velocity platform near Rydberg blockade. (d) Group velocity deviation ratio $\delta_v(Z)$ (see its definition in the text). For the same Z , more extending pulses have higher δ_v due to more spatially non-uniform interaction.

will be below the magnitude for realizing a significant XPM. Our results in Fig. 4 thus exclude the usefulness of the “head-on collision” (without transverse separation) considered in the previous studies [17–20].

The next target is to understand the real-time evolution of the DSP state $|1\rangle_1|1\rangle_2$ given before (1). In our concerned regime, the DSP propagation can be identified with that of the electromagnetic field, hence the kinetic Hamiltonian $H_K = -\sum_l i v_{g,l}(t) \int dz \hat{\Psi}_l^\dagger(z) \partial_z \hat{\Psi}_l(z)$ for the DSP fields. Meanwhile, for a slow light regime with $\cos\theta \ll 1$, the BSPs interact very slightly with the DSPs and among themselves because they contain negligible Rydberg excitation. Their quick decoupling from the system and damping into the environment allow one to treat the BSPs as motionless oscillations, though their group velocities can be read from their spectrum in (1).

Our method for pulse state evolution is to adopt the joint evolution $U(t, 0)$ as the time-ordered exponential $T e^{-i \int_0^t d\tau \{H(\tau) + H_D(\tau)\}}$ on the initial state $|\psi_{in}\rangle = |1\rangle_1|1\rangle_2|0\rangle_c$ as the product of the input pulse state and the reservoir vacuum state $|0\rangle_c$. Tracing out the reservoir degrees of freedom in the evolved state $U(t, 0)|\psi_{in}\rangle$

gives the evolved system state. We have three non-commutative items (H_K , H_{AF} and H_I) in $H(t)$, as well as the dissipation Hamiltonian $H_D(t)$ of (3), for the joint evolution operator $U(t, 0)$. Directly applying $U(t, 0)$ on the DSP operators in $|\psi_{in}\rangle$ is impossible, as it is equivalent to analytically solving a nonlinear Langevin equation. One technique to circumvent the difficulty is the factorization of an evolution operator into the relatively tractable ones [26]. For our problem we have $U(t, 0) = U_K(t, 0)U_{AF}(t, 0)U_I(t, 0)U_D(t, 0)$. Among the factorized processes $U_X(t, 0) = \text{T exp}\{-i \int_0^t d\tau \tilde{H}_X(\tau)\}$, for $X = K, AF, I$ and D , \tilde{H}_K and \tilde{H}_D are indifferent to their original form H_K and H_D , respectively. The operator $U_D(t, 0)$ takes no effect on $|\psi_{in}\rangle$, but the non-commutativity of H_D with H_{AF} makes the BSP field operators in H_{AF} become those in \tilde{H}_{AF} as follows:

$$\hat{\Phi}_{\pm, l}(z) \rightarrow \hat{\Xi}_{\pm, l}(z, \tau) = e^{-\phi_{\pm}^2 \gamma (t-\tau)/2} \hat{\Phi}_{\pm, l}(z) \pm \sqrt{\gamma} \phi_{\pm} \int_{\tau}^t dt' e^{-\phi_{\pm}^2 \gamma (t'-\tau)/2} \hat{\xi}_l(z), \quad (6)$$

where $\phi_{+(-)} = \cos \phi(\sin \phi)$. A sufficiently large γ approximates the commutator $[\hat{\Xi}_{\pm, l}(z, \tau_1), \hat{\Xi}_{\pm, l}^{\dagger}(z', \tau_2)] = e^{-\gamma \phi_{\pm} |\tau_1 - \tau_2|} \delta(z - z')$ as vanishing for $\tau_1 \neq \tau_2$. Under this approximation the BSP operators in $U_I(t, 0)$ also take the forms in (6), hence the transformation

$$\begin{aligned} \hat{U}_I^{\dagger}(t, 0) \hat{\Psi}_l(z) \hat{U}_I(t, 0) &= (\text{T} e^{ic_3^2 \int_0^t d\tau \hat{W}_l(z^{\tau}, \tau)})^{\dagger} \hat{\Psi}_l(z) \\ &- ic_3 \int_0^t d\tau (\text{T} e^{ic_3^2 \int_0^{\tau} dt' \hat{W}_l(z^{t'}, t')})^{\dagger} (c_1 \hat{\Xi}_{+, l}(z, \tau) \\ &+ c_2 \hat{\Xi}_{-, l}(z, \tau)) \hat{W}_l(z^{\tau}, \tau) \end{aligned} \quad (7)$$

to the first order of $\cos \theta$, with $c_1 = \cos \theta \sin \phi$, $c_2 = \cos \theta \cos \phi$, $c_3 = \sin \theta$, and $z^{\tau} = z + \int_0^{\tau} d\tau' v_{g, l}(\tau')$. The DSP operator picks up a phase from the term $\hat{W}_l(z, \tau) = \int dz' \Delta(z - z') \hat{\Pi}_{3-, l}^{\dagger} \hat{\Pi}_{3-, l}(z', \tau)$ ($\hat{\Pi}_l = c_1 \hat{\Xi}_{+, l} + c_2 \hat{\Xi}_{-, l} + c_3 \hat{\Psi}_l$), while this term constantly causes its transition to the BSP components along the time. Based on (7), the evolved state $\hat{U}_I(t, 0)|\psi_{in}\rangle$ (unnormalized) is found as

$$\begin{aligned} &\left\{ \int dz_1 dz_2 g(z_1, z_2) e^{-ic_3^4 \int_0^t d\tau \Delta(z_1^{\tau} - z_2^{\tau})} \hat{\Psi}_1^{\dagger}(z_1) \hat{\Psi}_2^{\dagger}(z_2) \right. \\ &- ic_3^3 \sum_{l=1}^2 \int_0^t d\tau \int dz_1 dz_2 g(z_1, z_2) e^{-ic_3^4 \int_0^{\tau} dt' \Delta(z_1^{t'} - z_2^{t'})} \\ &\times \Delta(z_1^{\tau} - z_2^{\tau}) (c_1 \hat{\Pi}_{+, l}^{\dagger} + c_2 \hat{\Pi}_{-, l}^{\dagger})(z_1, \tau) \hat{\Psi}_{3-, l}^{\dagger}(z_2) \left. \right\} |0\rangle_t, \end{aligned} \quad (8)$$

where $g(z_1, z_2) = f(z_1)f(z_2)$ and $|0\rangle_t = |0\rangle|0\rangle_c$. The succeeding operation U_{AF} only affects the BSP components in (8), while U_K displaces the coordinate of $\hat{\Psi}_l^{\dagger}(z_l)$. If the exact commutation relations for the BSPs in (6) are considered, the BSP part will take more complicated form, but it will not modify the DSP part, the first term of (8).

The interaction potential $\Delta(z_1 - z_2)$ renders the DSP part in (8) no longer factorizable with respect to z_1

and z_2 . This entangled piece deviates from the ideal output state $e^{i\varphi}|1\rangle_1|1\rangle_2$ with a uniform phase φ . We measure the degrees of such deviation by comparing the real output $|\psi_{out}\rangle = U(t, 0)|\psi_{in}\rangle$ with a reference state $|\psi_{out}^0\rangle = U_K(t, 0)U_{AF}(t, 0)U_D(t, 0)|\psi_{in}\rangle$. In the absence of $U_I(t, 0)$ this reference keeps to be in the product state $|1\rangle_1|1\rangle_2|0\rangle_c$ (the single DSP state $|1\rangle_l$, however, has the displaced spatial coordinate from its form at $t = 0$). The output's fidelity F with the ideal one and the associate cross phase φ can thus be found from the overlap $\sqrt{F}e^{i\varphi} = \langle \psi_{out}^0 | \psi_{out} \rangle$. Similar definitions for F and φ can be found in [27, 28].

In Fig. 5 we plot the fidelity and cross phase for the most transversely separated pulses in Fig.4. Due to the short range of VdW potential, both fidelity and cross phase for the counter-propagation in Fig.5(a) quickly converge to fixed values with increasing medium size. A cross phase of π rad that still keeps close to unit F could be achieved if the VdW coefficient $|C_6|$, for example, is lifted by about nine times with a different Rydberg level. Note that the high fidelity in counter-propagation has nothing to do with a widely held notion of spatially homogeneous interaction. The insertion of Fig.5(a) shows the fidelity for an imagined motion of two pulses passing each other very slowly. The same propagation geometry indicates that the degrading fidelity in the slow motion comes from the growing pulse entanglement over a longer interaction time. In comparison we also study the co-propagating pulses in Fig.5(b). The co-propagation exhibits considerable trade-off between F and φ , and would be unfavorable for making large phases of good quality.

In summary, we have studied the process of two-photon interaction via a Rydberg atomic ensemble. Our approach based on the complete dynamics for both single atoms and ensemble enables a more realistic description of the situation without steady state. The previously considered regime near Rydberg blockade is found to be short of the favorable figures of merit for photon-

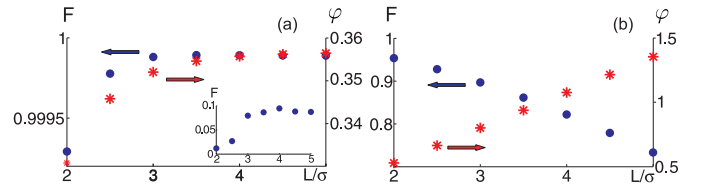


FIG. 5: (a) Fidelity and cross phase of photon-photon XPM for two counter-propagating pulses with the transverse separation $a = 1.5 \sigma$ in Fig.4. L is the medium size. The system parameters are the same as in Fig.4. The insertion describes an imagined situation by reducing the initial pulse velocity to 10^{-3} of that in Fig. 4. (b) Fidelity and cross phase for two pulses propagating together along two tracks separated by $a = 1.5 \sigma$. Due to pulse absorption, their group velocity is not stable in such co-propagation (for example, it drops from 11.007 m/s to 11.002 m/s from $L = 2\sigma$ to 5σ).

photon XPM, and the danger of entering the superluminal regime with tremendous dissipation should be avoided in practice. We also show that approximately ideal XPM creating considerable nonlinear phase can be realized with counter-propagating and transversely separated pulses that weakly interact with each other. Our methods and results may find applications to the quantum devices based on the similar processes.

B. H. and C. S. acknowledge the support by AITF and NSERC. M.X. acknowledges the support in part by NBRPC (Grants No. 2012CB921804). A. V. S. was supported by RFBR 12-02-31621.

* Electronic address: mxiao@uark.edu

- [1] H. Schempp, *et al*, Phys. Rev. Lett. 104, 173602 (2010).
- [2] J. D. Pritchard, D. Maxwell, A. Gauguier, K. J. Weatherill, M. P. A. Jones, and C. S. Adams, Phys. Rev. Lett. 105, 193603 (2010).
- [3] T. Peyronel, O. Firstenberg, Q.-Y. Liang, S. Hofferberth, A.V Gorshkov, T. Pohl, M. D. Lukin, and V. Vuletić, Nature (London) 488, 57 (2012).
- [4] Y. O. Dudin and A. Kuzmich, Science 336, 887 (2012).
- [5] D. Maxwell, *et al*, Phys. Rev. Lett. 110, 103001 (2013).
- [6] C. S. Hofmann, *et al*, Phys. Rev. Lett. 110, 203601 (2013).
- [7] O. Firstenberg, T. Peyronel, Q.-Y. Liang, A. V. Gorshkov, M. D. Lukin, and V. Vuletić, Nature (London) 502, 71 (2013).
- [8] C. Ates, S. Sevinçli, and T. Pohl, Phys. Rev. A 83, 041802(R) (2011).
- [9] S. Sevinçli, N. Henkel, C. Ates, and T. Pohl, Phys. Rev. Lett. 107, 153001 (2011).
- [10] D. Petrosyan, J. Otterbach, and M. Fleischhauer, Phys. Rev. Lett. 107, 213601 (2011).
- [11] J. D. Pritchard, C. S. Adams, and K. Mølmer, Phys. Rev. Lett. 108, 043601 (2012).
- [12] D. Yan, Y.-M. Liu, Q.-Q. Bao, C.-B. Fu, and J.-H. Wu, Phys. Rev. A 86, 023828 (2012).
- [13] D. Petrosyan and K. Mølmer, Phys. Rev. A 87, 033416 (2013).
- [14] M. Gärttner and J. Evers, Phys. Rev. A 88, 033417 (2013).
- [15] J. Otterbach, M. Moos, D. Muth, and M. Fleischhauer, Phys. Rev. Lett. 111, 113001 (2013).
- [16] J. Stanojevic, V. Parigi, E. Bimbard, A. Ourjoumteev, and P. Grangier, Phys. Rev. A 88, 053845 (2013).
- [17] I. Friedler, D. Petrosyan, M. Fleischhauer, and G. Kurizki, Phys. Rev. A 72, 043803 (2005).
- [18] B. He, A. MacRae, Y. Han, A. Lvovsky, and C. Simon, Phys. Rev. A 83, 022312 (2011).
- [19] E. Shahmoon, G. Kurizki, M. Fleischhauer, and D. Petrosyan, Phys. Rev. A 83, 033806 (2011).
- [20] A. V. Gorshkov, J. Otterbach, M. Fleischhauer, T. Pohl, and M. D. Lukin, Phys. Rev. Lett. 107, 133602 (2011).
- [21] M. Fleischhauer and M. D. Lukin, Phys. Rev. Lett. 84, 5094 (2000).
- [22] C. W. Gardiner and P. Zoller, *Quantum Noise* (Springer-Verlag, Berlin, 2000).
- [23] J. Gea-Banacloche, Y. Li, S. Jin, and M. Xiao, Phys. Rev. A 51, 576 (1995).
- [24] The superluminal regime is in the order of EIT linewidth from $\Delta_R = 0$, see Fig. 3(b). To a multi-photon beam, immediate loading Δ_R much larger than the EIT linewidth directly pushes a local atom into the blockade regime, irrespective of the sign of Δ_R .
- [25] L. Béguin, A. Vernier, R. Chicireanu, T. Lahaye, and A. Browaeys, Phys. Rev. Lett. 110, 263201 (2013).
- [26] B. He, Phys. Rev. A 85, 063820 (2012).
- [27] J. Gea-Banacloche, Phys. Rev. A 81, 043823 (2010).
- [28] B. He and A. Scherer, Phys. Rev. A 85, 033814 (2012).